



Exploring a new method to obtain the 3D abrasive water jet profile

Shijin Zhang¹ · Lidanyang Ji¹ · Yuqiang Wu^{1,2} · Ming Chen¹ · Wenkang Zhou¹

Received: 2 October 2019 / Accepted: 6 March 2020 / Published online: 7 May 2020
© Springer-Verlag London Ltd., part of Springer Nature 2020

Abstract

As high-pressure water combined with abrasive particles together comes out from a nozzle, a high-energy abrasive water jet beam is formed. And this high-energy water jet beam could be used as a sharp knife to cut all types of material. Different from a rigid knife, whose profile is fixed, this high-energy beam's profile is changing as the cutting parameters change. Therefore, if this knife is used to cut a workpiece accurately and precisely, the knife's profile under each set of cutting conditions has to be searched out. And further, based on the jet profile, compensation on the jet profile has to be carried out. In the past, a 2D model for the kerf profile cut by jet has been built; then, compensation on the jet based on the 2D model of the kerf profile has been carried out. However, using a 2D model to describe a 3D profile is definitely not enough. In this paper, a new method generating a 3D kerf profile through scanning an integrated sample has been provided. With this method, complete 3D abrasive water jet profiles under each cutting conditions could be obtained through the kerf profiles. With these precise 3D abrasive water jet profiles, better compensating the cutting errors becomes possible in future.

Keywords AWJ · 3D model of jet profile · Kerf profile · Scanning · Curve fitting

1 Introduction

Abrasive water jet (AWJ) cutting is a process in which water is pressurized to a very high pressure by a high-pressure pump. The pressurized water is then forced out from a very small nozzle, and a high-speed water jet beam is formed [1]. This high-speed water jet beam can be used to cut all kinds of materials. As a cold working process, AWJ has some special advantages, such as no heat effect, high efficiency, and environmental friendliness [2]. Therefore, this technology has been used widely in many industry fields. However, this potential cutting technology has been blocked in some precision manufacturing processes because it leads to some defects on the cutting surface. For example, this high-energy water jet beam would dissipate as it penetrates the material. When the energy depletes

along the thickness direction, the cutting ability of the jet degrades [3]. As a result, some unacceptable characteristics, such as rough and striated kerf surface, as shown in Fig. 1, jet lag, as shown in Fig. 2, and distorted kerf geometry, as shown in Fig. 3, would be present on the samples cut by AWJ. These defects have seriously hindered AWJ for wider applications.

In order to eliminate these defects, researchers from the whole world have put a lot of efforts on it. Based on the results of their research, two methods could be used to eliminate those defects. The first method is adjusting the traversing speed of the nozzle. As is well known, the surface cut by AWJ could be very smooth as the nozzle traversing speed becomes very low. Based on Zeng J. [6], during AWJ cutting process, the cutting surface roughness is highly related to the nozzle traversing speed. He used 5 different cutting surface quality levels to describe the cutting surface roughness, as shown in Fig. 4. Quality 1 corresponds to a very high nozzle traversing speed, and quality 5 corresponds to a low nozzle traversing speed. Therefore, by slowing down the nozzle traversing speed, very smooth cutting surface could be obtained. And also, by slowing down the nozzle traversing speed, jet lag could also be improved greatly. Actually, kerf geometry could also be changed by adjusting the nozzle traversing speed, as shown in Fig. 5.

✉ Yuqiang Wu
knightstrike@hotmail.com

¹ Shanghai Key Lab of Intelligent Manufacturing and Robotic, School of Mechatronic Engineering and Automation, Shanghai University, Shanghai 200072, China

² School of Mechanical Engineering, Xihua University, Chengdu 610039, China

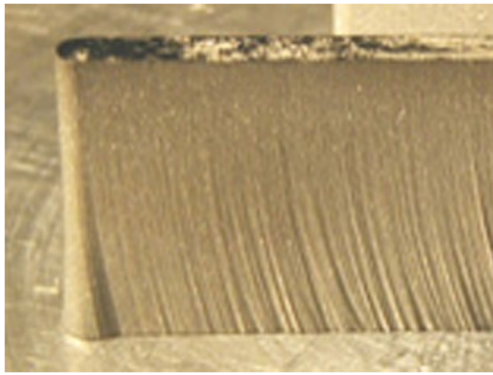


Fig. 1 Sample with rough and striated kerf surface cut by AWJ [1]

Another method which could be used to eliminate the natural defects of AWJ cutting is using a 5-axis waterjet cutting head, as shown in Fig. 6.

By adjusting the cutting head to a proper tilting angle, the natural defects could be eliminated, as shown in Fig. 7.

Comparing these two methods, without a doubt, in most cases, the first method is not acceptable since it is with very low efficiency. And the second method is a very effective way. Therefore, in the last 20 years, many researchers have worked on this method. Obviously, for a complicated contour, to eliminate the natural defects of AWJ cutting, a proper tilting angle has to be found first on each cutting spot. And logically, the error compensation strategy is based on knowing the abrasive water jet profiles precisely. Therefore, searching the jet profile, and further searching the cutting head controlling strategy, is the most effective way to eliminate AWJ cutting defects.

As we know, jet profile might be completely different as the jet ejects into different media. For example, when jet ejects into air, the jet profile is more like a pyramid, as shown in Fig. 8. However, as the jet cuts into one kind of material, the jet profile is completely different, as shown in Fig. 9. Actually, as the jet cuts into a workpiece, its profile might change dynamically since it is affected by many factors, such as the material type, thickness of the material, nozzle combination, and nozzle traversing velocity. And during cutting process, the jet profile could be represented by the kerf profile. Therefore, a better way to investigate the jet profile during cutting process is to investigate the kerf profile.



Fig. 2 Jet lag of AWJ [4]

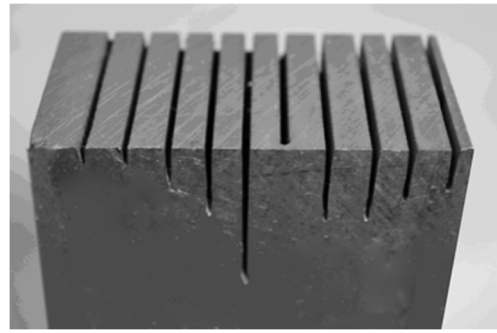


Fig. 3 Distorted kerf geometry cut by AWJ [5]

In the past 20 years, many researchers have worked on kerf profile investigation. In 2004, Ma C. and Deam R.T. [9] investigated the kerf geometry of acrylic plastic by using an optical microscope. In 2008, Shanmugam et al. [10] measured the kerf taper angles on the two kerf walls. Based on the measurement, he developed a predictive model for the kerf taper angle by using a dimensional analysis technique. In 2009, Shanmugam D. K. and Masood S. H. [11] investigated the kerf taper angle by using an optical microscope. In 2009, to study the influence of the jet impingement angle and jet feed rate on the kerf generation in AWJ machining, Srinivasu, D. S. et al. [12] used a fiber-optic digital microscope to analyze the cut surfaces. In 2014, Gupta, V. et al. [13] investigated the kerf characteristics of the marble cut by AWJ through measuring the kerf taper, top kerf width and depth of cut. In 2015, in order to obtain the accurate kerf profiles, Wang, S. et al. [14, 15] used a dial indicator to measure the contour of the kerf profile at a series of equally spaced points along the marked lines, as shown in Fig. 10.

In 2016, Pahuja, R. et al. and Ramulu, M. and Isvilanonda, V. [16, 17] investigated the machinability of thermoplastic titanium graphite (TiGr) FML. The feasibility and machinability of the thick (7.6–10.5 mm) TiGr through AWJ process were studied in terms of machined kerf characteristics—taper ratio and surface quality. These characteristics were

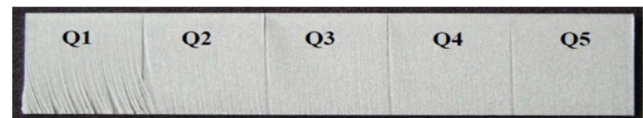
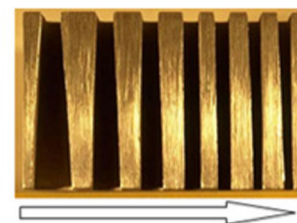


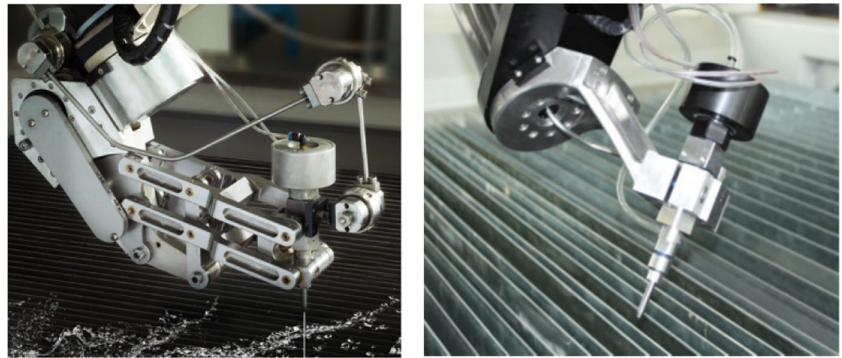
Fig. 4 Samples cut by AWJ with 5 surface quality levels [7]



Nozzle traversing speed increased gradually

Fig. 5 Kerf geometry changes as the traversing speed changes [8]

Fig. 6 AWJ 5-axis cutting head



revealed by SEM inspection, optical microscope, and surface profilometry. Predictive mathematical regression models were developed through analysis of variance (ANOVA) in order to optimize the process. In 2019, Pahuja R. and Ramulu M. [18] investigated the material removal mechanisms by using a scanning electron microscope. Based on the above research, the taper angle has been defined for some material with different thicknesses.

Except taper, jet lag is another reason of caused defects in AWJ cutting process. In order to eliminate jet lag, many researchers also spent a lot of time to work on it. In 2010, to identify the cutting front geometry, Akkurt A. [19] made some samples with AWJ machine and separated them with a milling machine to observe the cutting front geometry of AWJ. Finally, the cutting front geometry was characterized by a second-degree polynomial equation as a parabolic function. In 2015, Zhang, S. et al. [20] used a new method, in which the abrasive feeding hose from the nozzle side had been pulled off during the stable cutting phase, to cut off the supply of abrasive in a very short period of time. By this way, the real cutting front corresponding to the cutting parameters had been obtained. After that, a dial indicator with a rigid needle fixed on it had been used to measure the cutting front. By recording 25 points on each cutting front, the cutting front profile has

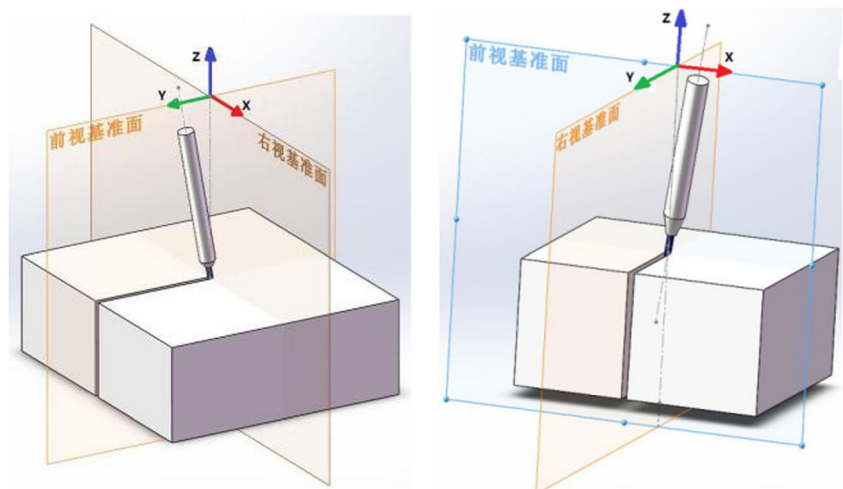
been obtained. In 2019, Mital, G. et al. [21] used a 3D laser profilometer to measure the roughness of the kerf surface of AWJ and created a 3D image of one-side kerf surface.

Based on the above researches, it seems the kerf profile could be obtained successfully. However, almost all kerf profiles obtained above are based on 2D models. As a result, the cutting front was described as a parabolic curve. And the taper was also described as two curves. As we know, the kerf profile is a 3D profile definitely. Describing this 3D profile using a 2D profile would lose some important characteristics, further affecting the defect-eliminating process. In order to obtain the kerf profile with more details, a method has been explored to build a 3D model of abrasive water jet kerf profile.

2 Making samples for 3D kerf profile investigation

In order to make samples for kerf profile investigation, a traditional way is cutting a selected sample under a set of specified conditions, as shown in Fig. 11. After cutting is finished, the samples were separated into two halves. Therefore, each half could be used for investigation. The good side of this method is that it is very easy to make samples. The bad side

Fig. 7 Eliminating the natural defects by tilting the cutting head a small angle along two directions [4]



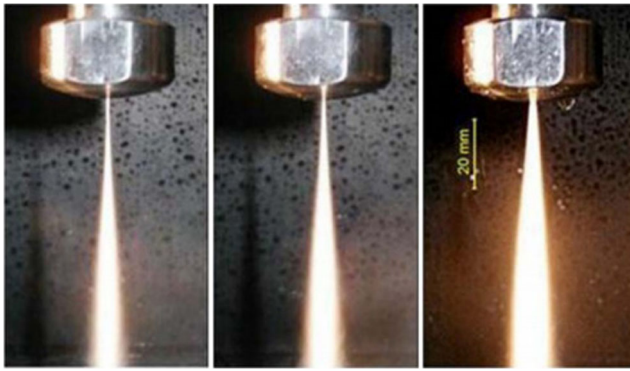


Fig. 8 Jet profile as jet ejects into air [4]

of it is that some characteristics of the kerf profile could not be kept completely. Obviously, to obtain a complete 3D kerf profile, the above way is unacceptable. Another new method needs to be searched out.

2.1 A new method to make raw samples for cutting

As mentioned above, with traditional way to make sample, the kerf would be damaged during the separation process. In that case, a complete 3D kerf profile could not be obtained. In order to obtain a complete 3D kerf profile, two blocks with the same dimensions, instead of one block, have been made. And these two blocks are integrated tightly, as shown in Fig. 12.

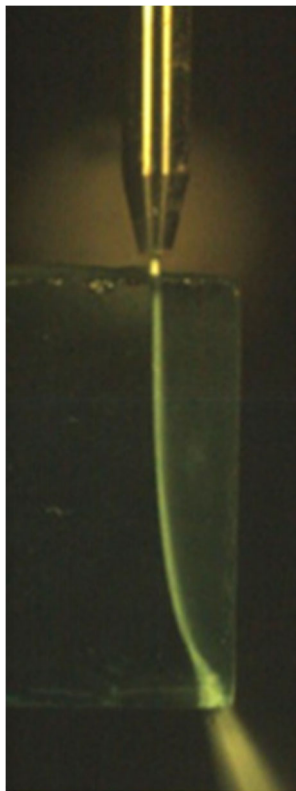


Fig. 9 Jet profile as jet cuts into glass [1]

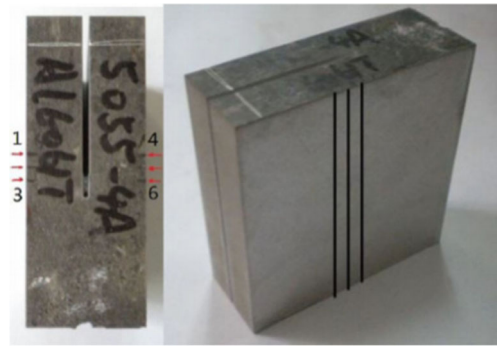


Fig. 10 Measurement of the kerf profile [15]

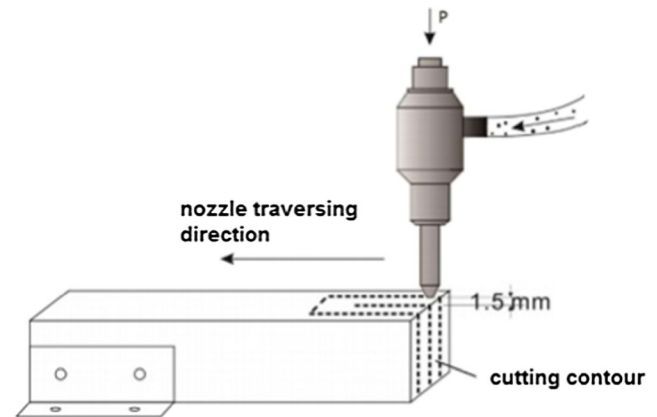


Fig. 11 Traditional method to make sample for investigation

Before using this new method as a method to make sample, one thing needs to be done firstly is to ensure that the mechanical properties of the sample are consistent with the original material. In order to verify that, several cuts under the same cutting conditions had been conducted on the integrated samples and whole-piece samples respectively. The cutting conditions are listed in Table 1. After cutting, the cutting front and the taper had been compared, as shown in Fig. 13. Based on the comparison, as long as the requirements for the integrated samples are satisfied, the integrated sample had the same characteristics as the whole-piece sample. The requirements for the integrated sample are shown in Fig. 14.

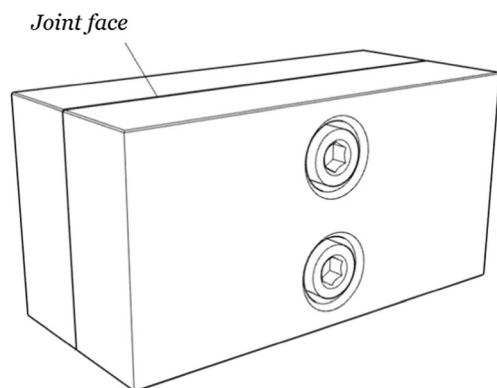


Fig. 12 Integrating two blocks together for cutting

Table 1 AWJ cutting parameters

Experimental parameters	Specifications
Pressure inside the pumping system	350 MPa
Abrasive mass flow rate	0.5 kg/min
Abrasive material average grain size	0.250 mm (80 mesh)
Abrasive material type	Garnet
Water orifice diameter	0.33 mm
Focusing tube diameter	0.889 mm
Stand-off distance	1.5 mm
Material	Aluminum/carbon steel
Material thickness	30 mm
Traverse velocity	Aluminum: 288.38 /259.9/163.04/117.12/90.61 mm/min Carbon steel: 106.91/96.35/60.44/43.42/33.59 mm/min

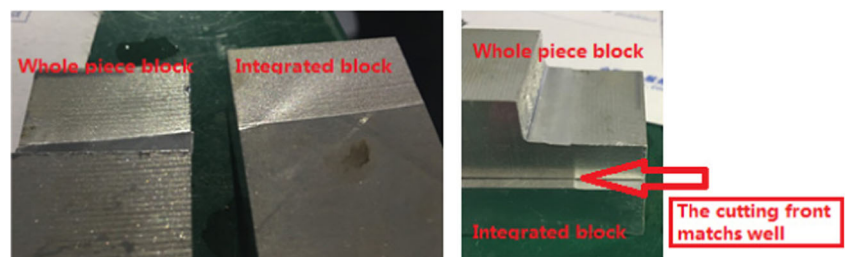
In order to let these two blocks integrate together tightly, the joint faces of the two blocks have to be very smooth (the roughness of the surface is equal or less than 0.8μm). Besides, some requirements have to be satisfied, as shown in Fig. 14.

2.2 Sample-making process on integrated blocks

After verifying the effectiveness of this new method, some samples need to be made for jet profile investigation. In order to make samples needed, carbon steel has been selected as the target material for cutting. The AWJ cutting parameters are listed in Table 2.

Some explanations are needed for Table 2. In Table 2, most parameters are fixed. The reason for that is the purpose of this investigation is exploring a method to obtain complete 3D kerf profiles. Therefore, there is no need to carry out a full-factor experiment. Except that, the traversing velocity in Table 1 is listed as surface quality levels instead. In this experiment, in order to get a stable traversing velocity phase, a 50-mm long kerf has been cut for each sample. And the nozzle traversing velocity is calculated based on a separating speed. The separating speed is obtained based on cutting experiments [7]. From the separating experiments, the separating speed for 40-mm-thick carbon steel is 67.40 mm/min. After obtaining the separating speed, the other traversing velocities corresponding to different surface quality levels in Table 2 could be calculated according to Zeng's model [6].

Fig. 13 The cutting kerf comparison of the integrated sample and the whole-piece sample



$$u = \left(\frac{N_m P_w^{1.25} \dot{m}_w^{0.687} \dot{m}^{0.343}}{C_s q h D^{0.618}} \right)^{1.15} \quad (1)$$

where u represents the nozzle traversing velocity (mm/s); N_m represents the machinability number of material; \dot{m}_w represents the waterflow rate (lpm); \dot{m} represents the abrasive flow rate (g/s); P_w represents the water pressure (MPa); C_s represents the scale factor; q represents the surface quality level; D represents the mixing tube diameter (mm); and h represents the thickness of sample (mm).

From Eq. (1), the traversing speeds corresponding to different surface quality levels could be calculated as follows: $u(Q_1) = 67.40$ mm/min; $u(Q_2) = 30.37$ mm/min; $u(Q_3) = 19.05$ mm/min; $u(Q_4) = 13.69$ mm/min; $u(Q_5) = 10.59$ mm/min.

The cutting process for the integrated sample is shown in Fig. 15. After cutting, the integrated sample is shown in Fig. 16.

3 D kerf profile generation

After cutting, the kerf has been generated. By taking the two integrated blocks apart, the kerf profile could be obtained without any damage, as shown in Fig. 17.

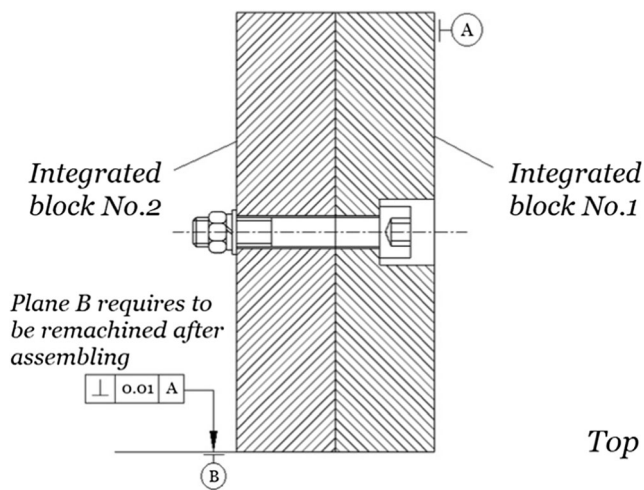


Fig. 14 The machining requirement for each integrated block

Table 2 AWJ cutting parameters

Experimental parameters	Specifications
Pressure inside the pumping system	330 MPa
Abrasive mass flow rate	0.45 kg/min
Abrasive material average grain size	0.250 mm (80 mesh)
Abrasive material type	garnet
Water orifice diameter	0.33 mm
Focusing tube diameter	0.889 mm
Stand-off distance	1.5 mm
Material	Carbon steel
Material thickness	40 mm
Traverse velocity	$u(Q_1) u(Q_2) u(Q_3) u(Q_4) u(Q_5)$

3.1 Building point cloud model for the integrated sample through scanning

In order to obtain the 3D kerf profile, a high-precision hand-held 3D laser scanner, as shown in Fig. 18, has been used to obtain the cloud point data of the integrated

samples. The parameters of the hand-held 3D laser scanner are listed in Table 3.

Logically, for scanning, the two integrated blocks need to be taken apart. After scanning, to build a 3D kerf profile model, those two blocks need to be integrated again. To work on this process, several steps need to be followed. Firstly, selecting several planes as reference surfaces, as shown in Fig. 19.

After scanning, thousands of points have been generated for each plane. Since those points cannot be used directly, several fitting planes have been generated based on those points scanned from each original plane, as shown in Fig. 20.

Now, it is the time to integrate these planes together. Theoretically, by setting joint face of block 1 and joint face 2 of block 2 as one surface, then by putting plane B of block 1 and plane B2 of block 2 in the same plane, and also by putting plane C of block 1 and plane C2 of block 2 in the same plane, the two joint planes could be integrated together. Need to note that, because of some scanning errors and surface fitting errors, adjustment needs to be carried out. After integrating, the 3D kerf profile could be obtained, as shown in Fig. 21.

3.2 Extracting the kerf profile through the integrated sample built from scanned point cloud

In order to extract the kerf profile at any cutting point, a coordinate system has been built, as shown in Fig. 22. For this coordinate system, the joint face of the two blocks was selected as XY plane. And B-B2 plane was selected as YZ plane. The bottom plane of the integrated sample was selected as XZ plane.

As shown in Fig. 23, to extract the kerf profile at each cutting point, a plane which is not only through that point but also parallel to YZ plane had been built. Then, the intersection curves between the plane and the kerf have been searched out. By this way, a series of kerf profiles could be obtained. Table 4 listed four sets of the kerf wall curves extracted.

Fig. 15 The AWJ cutting process for the integrated sample



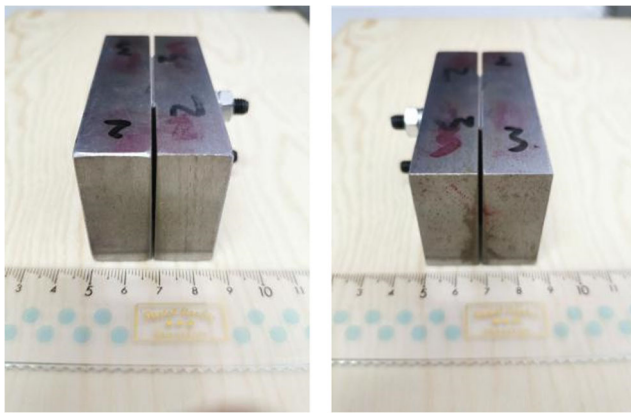


Fig. 16 Integrated samples after cutting

After putting these 4 sets of kerf wall curves together, the results are shown in Fig. 24.

As shown in Fig. 24, the kerf side wall curves extracted from cutting spots $X=7.5$, $X=10$, and $X=12.5$ are extraordinarily similar. However, the kerf side wall curve extracted from cutting spot $X=2$ is different. The reason for that is that the traversing velocity at cutting spot $X=2$ is different from the traversing velocities of those other three cutting spots. This further demonstrates that different traversing velocities would lead to different kerf profiles.

Through the same way, the cutting front curves could be extracted, as shown in Fig. 25. And the curves extracted are listed in Table 5.

After putting all three cutting front curves together, the results are shown in Fig. 26.



Fig. 17 The cutting surface of the integrated sample



Fig. 18 Hand-held 3D scanner

As shown in Fig. 26, the three cutting front curves have the same trend though the spatial locations of them are different.

4 Conclusions

The above contents lead to the following conclusions:

1. By integrating two blocks together tightly, then by using AWJ to cut the integrated sample along the joint face of these two blocks, the complete kerf profile had been obtained. This method provided a new way to obtain kerf profile without any damage.
2. By using a high-precision hand-held 3D laser scanner to scan the kerf profile, then by following some specified fitting rules, a 3D kerf profile, which is based on scanned point cloud, had been generated.
3. By building a series of planes which intersect with the 3D kerf profile model, a series of kerf side wall curves and cutting front curves had been extracted. According to these curves, the kerf side wall profile changes as the nozzle traversing velocity changes.

Through this method, complete 3D abrasive water jet profiles under each cutting conditions could be obtained through the kerf profiles. With these precise 3D abrasive water jet

Table 3 The parameters of the Holon 380

Parameters	Specifications
Scanning range (m)	0.1–10
Scanning accuracy (mm/m)	± 0.02
Resolution rate (mm)	0.05

Fig. 19 The reference planes selected for each integrated block

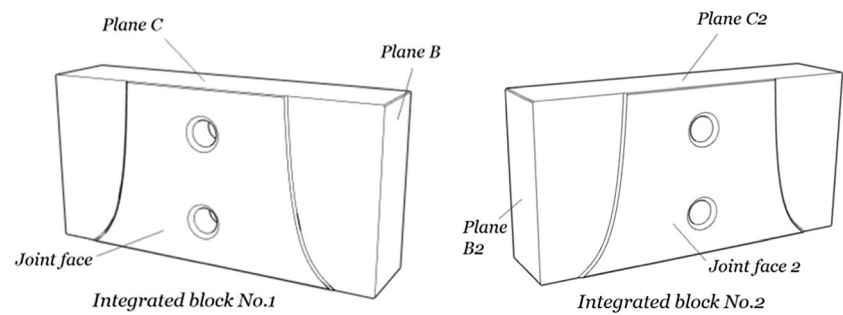


Fig. 20 Fitting planes built from the point cloud

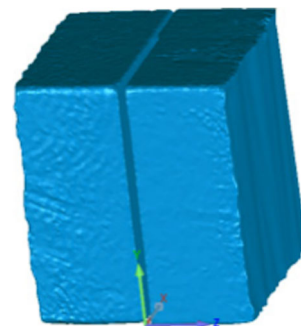
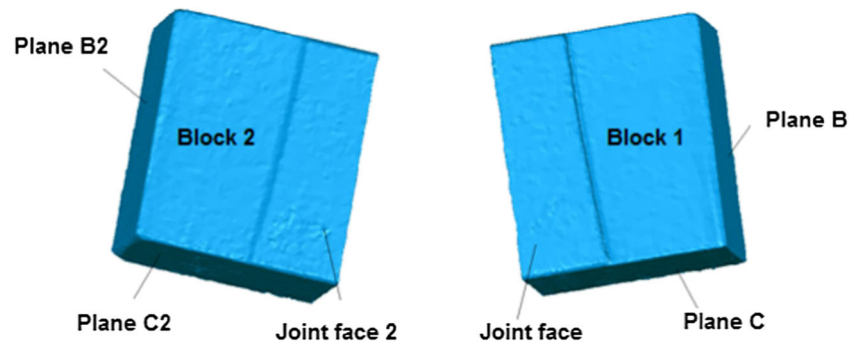


Fig. 22 The kerf profile with coordinate system



Fig. 21 Integrated sample built from scanned point cloud

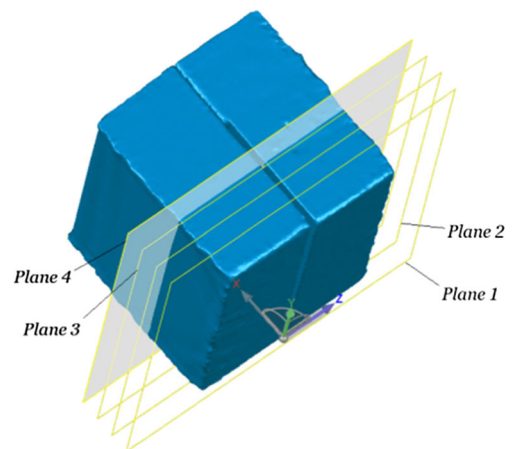
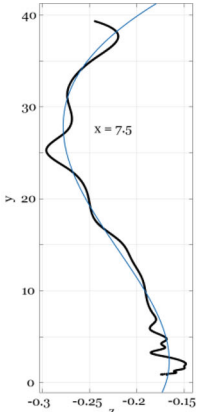
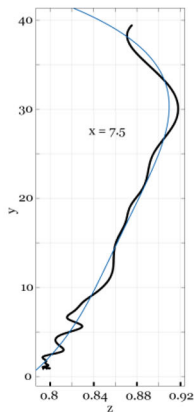
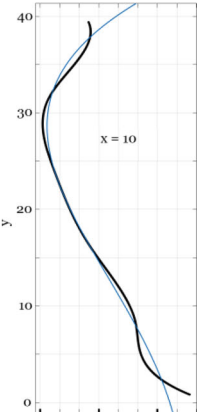
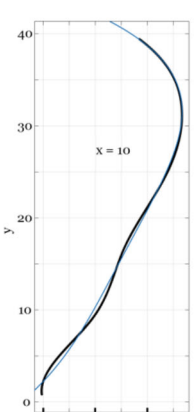
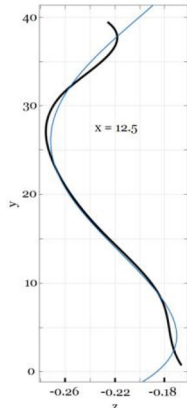
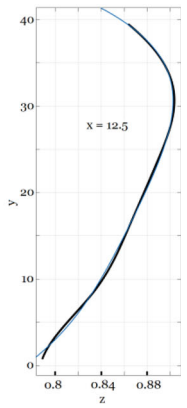
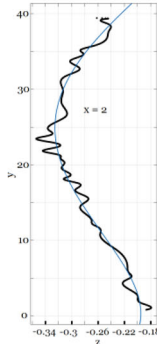
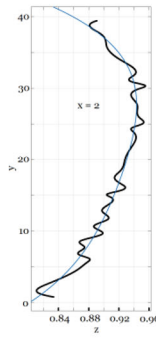


Fig. 23 Extracting the kerf profile at different cutting points

Table 4 Extracted kerf wall curves corresponding to Q4 traversing velocity

Kerf wall curve (left side)	Kerf wall curve (right side)
 <p>Corresponding to plane 2 through x=7.5 cutting spot</p>	 <p>Corresponding to plane 2 through x=7.5 cutting spot</p>
$f(y) = -0.00000009273 \cdot y^4 + 0.00001907 \cdot y^3 - 0.0007088 \cdot y^2 + 0.003055 \cdot y - 0.1694$ <p>Goodness of fit: SSE: 0.1768 R2: 0.955 RMSE: 0.008479</p>	$f(y) = -0.0000003748 \cdot y^4 + 0.00002411 \cdot y^3 - 0.0005691 \cdot y^2 + 0.009799 \cdot y + 0.7803$ <p>Goodness of fit: SSE: 0.07791 R2: 0.9736 RMSE: 0.005621</p>
 <p>Corresponding to plane 3 through x=10 cutting spot</p>	 <p>Corresponding to plane 3 through x=10 cutting spot</p>
$f(y) = 0.00000007438 \cdot y^4 + 0.0000026 \cdot y^3 - 0.0001783 \cdot y^2 - 0.003163 \cdot y - 0.1473$ <p>Goodness of fit: SSE: 0.07055 R2: 0.9816 RMSE: 0.005317</p>	$f(y) = -0.0000002795 \cdot y^4 + 0.00001819 \cdot y^3 - 0.0004379 \cdot y^2 + 0.008396 \cdot y + 0.7832$ <p>Goodness of fit: SSE: 0.01048 R2: 0.9964 RMSE: 0.002049</p>

 <p>Corresponding to plane 4 through x=12.5 cutting spot</p>	 <p>Corresponding to plane 4 through x=12.5 cutting spot</p>
$f(y) = -0.0000004065 \cdot y^4 + 0.0000435 \cdot y^3 - 0.001313 \cdot y^2 + 0.008594 \cdot y - 0.1863$ <p>Goodness of fit: SSE: 0.04762 R2: 0.9851 RMSE: 0.004369</p>	$f(y) = -0.0000002818 \cdot y^4 + 0.00001899 \cdot y^3 - 0.0005082 \cdot y^2 + 0.01005 \cdot y + 0.7738$ <p>Goodness of fit: SSE: 0.05546 R2: 0.998 RMSE: 0.001491</p>
 <p>Corresponding to plane 1 through x=2 cutting spot</p>	 <p>Corresponding to plane 1 through x=2 cutting spot</p>
$f(y) = -0.0000003053 \cdot y^4 + 0.00003306 \cdot y^3 - 0.0008664 \cdot y^2 + 0.0005416 \cdot y - 0.1949$ <p>Goodness of fit: SSE: 0.193 R2: 0.9576 RMSE: 0.008797</p>	$f(y) = -0.0000003651 \cdot y^4 + 0.00002555 \cdot y^3 - 0.0007615 \cdot y^2 + 0.01438 \cdot y + 0.8013$ <p>Goodness of fit: SSE: 0.1174 R2: 0.9609 RMSE: 0.006858</p>

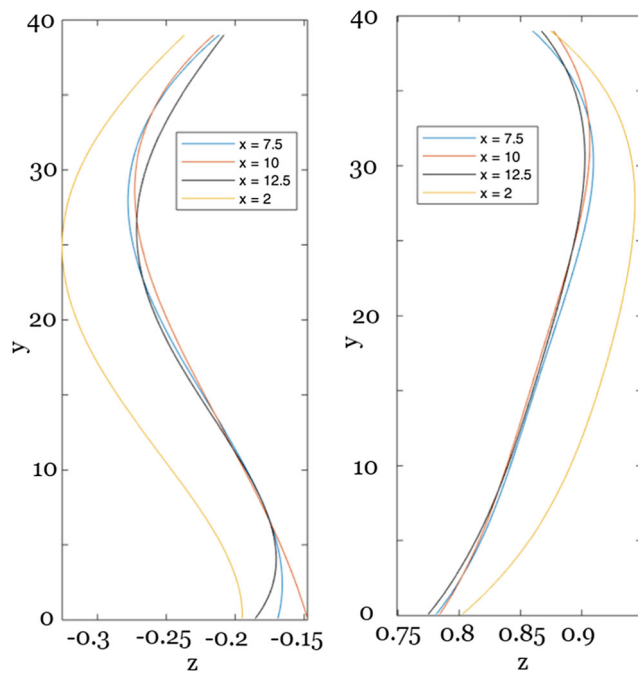


Fig. 24 All 4 sets of kerf side wall curves together

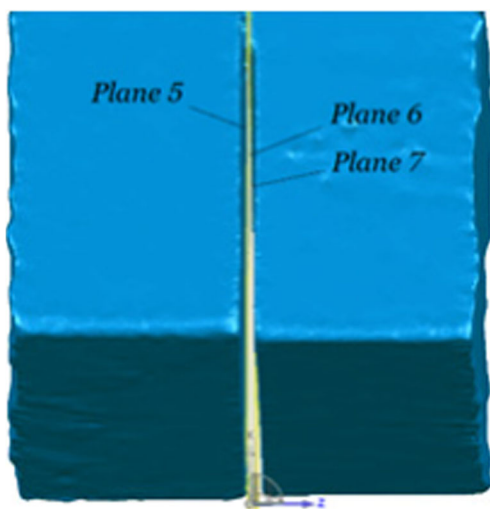
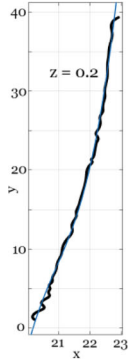
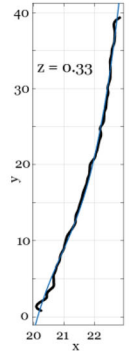
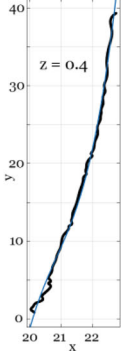
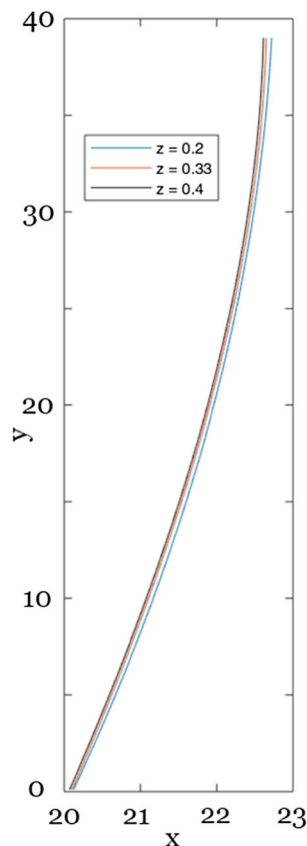


Fig. 25 Extracting the cutting front profile at different cutting points

Table 5 Cutting front of Q4

Cutting front	Cutting front	Cutting front
 <p>Corresponding to plane 5 through $z=0.2$ cutting spot</p>	 <p>Corresponding to plane 6 through $z=0.33$ cutting spot</p>	 <p>Corresponding to plane 7 through $z=0.4$ cutting spot</p>
$f(y) = -0.000001412 \cdot y^3 - 0.001271 \cdot y^2 + 0.1186 \cdot y + 20.11$ Goodness of fit: SSE: 7.932 R ² : 0.9971 RMSE: 0.04003	$f(y) = -0.000009167 \cdot y^3 - 0.0007905 \cdot y^2 + 0.1104 \cdot y + 20.09$ Goodness of fit: SSE: 8.104 R ² : 0.9971 RMSE: 0.04028	$f(y) = -0.000009608 \cdot y^3 - 0.0007782 \cdot y^2 + 0.1104 \cdot y + 20.06$ Goodness of fit: SSE: 10.23 R ² : 0.9963 RMSE: 0.04525

**Fig. 26** All three cutting front curves together

profiles, better compensating the cutting errors becomes possible in future.

Funding information This work was supported by the National Natural Science Foundation of China (Grant No. 51675320) and the Scientific Research Fund of Sichuan Provincial Education Department (Grant No. 18ZA0451).

References

- Chen M, Zhang S, Zeng J, Chen B, Xue J, Ji L (2019) Correcting shape error on external corners caused by the cut-in/cut-out process in abrasive water jet cutting. *Int J Adv Manuf Technol* 103(1–4): 849–859
- Chen M, Zhang S, Zeng J, Chen B (2018) Correcting shape error located in cut-in/cut-out region in abrasive water jet cutting process. *Int J Adv Manuf Technol* 102:1165–1178
- Arola D, Ramulu M (1997) Material removal in abrasive waterjet machining of metals surface integrity and texture. *Wear* 210:50–58
- Chen B (2019) Research on non-destructive precision cutting mechanism of abrasive jet. Dissertation. (in Chinese)
- Geng P (2012) The research of high pressure waterjet cutting process parameters. Dissertation. (in Chinese)
- Zeng J (1992) Mechanisms of brittle material erosion associated with high pressure abrasive waterjet processing - a modeling and application study. Dissertation
- Zeng J (2007) Determination of machinability and abrasive cutting properties in AWJ cutting. In 2007 American Waterjet WJTA Conference. Houston, Texas

8. Hashish M (2004) Precision cutting of thick materials with AWJ. In: BHR group 2004 water jetting, 33–46
9. Ma C, Deam RT (2006) A correlation for predicting the kerf profile from abrasive water jet cutting. *Exp Thermal Fluid Sci* 30(4):337–343
10. Shanmugam DK, Wang J, Liu H (2008) Minimisation of kerf tapers in abrasive waterjet machining of alumina ceramics using a compensation technique. *Int J Mach Tools Manuf* 48(14):1527–1534
11. Shanmugam DK, Masood SH (2009) An investigation on kerf characteristics in abrasive waterjet cutting of layered composites. *J Mater Process Technol* 209(8):3887–3893
12. Srinivasu DS, Axinte DA, Shipway PH, Folkes J (2009) Influence of kinematic operating parameters on kerf geometry in abrasive waterjet machining of silicon carbide ceramics. *Int J Mach Tools Manuf* 49(14):1077–1088
13. Gupta V, Pandey PM, Garg MP, Khanna R, Batra NK (2014) Minimization of kerf taper angle and kerf width using Taguchi's method in abrasive water jet machining of marble. *Procedia Mater Sci* 6(Icmpc):140–149
14. Wang S, Zhang S, Wu Y, Yang F (2017) A key parameter to characterize the kerf profile error generated by abrasive water-jet. *Int J Adv Manuf Technol* 90(5–8):1265–1275
15. Wang S, Zhang S, Wu Y, Yang F (2017) Exploring kerf cut by abrasive waterjet. *Int J Adv Manuf Technol* 93(5–8):2013–2020
16. Pahuja R, Ramulu M, Hashish M (2016) Abrasive waterjet profile cutting of thick titanium/graphite fiber metal laminate. *Adv Manuf* 2(November):V002T02A013
17. Ramulu M, Isvilanonda V, Pahuja R, Hashish M (2016) Experimental investigation of abrasive waterjet machining of titanium graphite laminates. *Int J Autom Technol* 10(3):392–400
18. Pahuja R, Ramulu M (2019) Abrasive water jet machining of titanium (Ti6Al4V)–CFRP stacks – a semi-analytical modeling approach in the prediction of kerf geometry. *J Manuf Process* 39(March):327–337
19. Akkurt A (2010) Cut front geometry characterization in cutting applications of brass with abrasive water jet. *J Mater Eng Perform* 19(4):599–606
20. Zhang S, Wu Y, Wang S (2015) An exploration of an abrasive water jet cutting front profile. *Int J Adv Manuf Technol* 80(9–12):1685–1688
21. Mital G, Dobránský J, Ružbarský J, Olejárová Š (2019) Application of laser profilometry to evaluation of the surface of the workpiece machined by abrasive waterjet technology. *Appl Sci (Switzerland)* 9(10)

Publisher's note Springer Nature remains neutral with regard to jurisdictional claims in published maps and institutional affiliations.

Terms and Conditions

Springer Nature journal content, brought to you courtesy of Springer Nature Customer Service Center GmbH (“Springer Nature”).

Springer Nature supports a reasonable amount of sharing of research papers by authors, subscribers and authorised users (“Users”), for small-scale personal, non-commercial use provided that all copyright, trade and service marks and other proprietary notices are maintained. By accessing, sharing, receiving or otherwise using the Springer Nature journal content you agree to these terms of use (“Terms”). For these purposes, Springer Nature considers academic use (by researchers and students) to be non-commercial.

These Terms are supplementary and will apply in addition to any applicable website terms and conditions, a relevant site licence or a personal subscription. These Terms will prevail over any conflict or ambiguity with regards to the relevant terms, a site licence or a personal subscription (to the extent of the conflict or ambiguity only). For Creative Commons-licensed articles, the terms of the Creative Commons license used will apply.

We collect and use personal data to provide access to the Springer Nature journal content. We may also use these personal data internally within ResearchGate and Springer Nature and as agreed share it, in an anonymised way, for purposes of tracking, analysis and reporting. We will not otherwise disclose your personal data outside the ResearchGate or the Springer Nature group of companies unless we have your permission as detailed in the Privacy Policy.

While Users may use the Springer Nature journal content for small scale, personal non-commercial use, it is important to note that Users may not:

1. use such content for the purpose of providing other users with access on a regular or large scale basis or as a means to circumvent access control;
2. use such content where to do so would be considered a criminal or statutory offence in any jurisdiction, or gives rise to civil liability, or is otherwise unlawful;
3. falsely or misleadingly imply or suggest endorsement, approval, sponsorship, or association unless explicitly agreed to by Springer Nature in writing;
4. use bots or other automated methods to access the content or redirect messages
5. override any security feature or exclusionary protocol; or
6. share the content in order to create substitute for Springer Nature products or services or a systematic database of Springer Nature journal content.

In line with the restriction against commercial use, Springer Nature does not permit the creation of a product or service that creates revenue, royalties, rent or income from our content or its inclusion as part of a paid for service or for other commercial gain. Springer Nature journal content cannot be used for inter-library loans and librarians may not upload Springer Nature journal content on a large scale into their, or any other, institutional repository.

These terms of use are reviewed regularly and may be amended at any time. Springer Nature is not obligated to publish any information or content on this website and may remove it or features or functionality at our sole discretion, at any time with or without notice. Springer Nature may revoke this licence to you at any time and remove access to any copies of the Springer Nature journal content which have been saved.

To the fullest extent permitted by law, Springer Nature makes no warranties, representations or guarantees to Users, either express or implied with respect to the Springer nature journal content and all parties disclaim and waive any implied warranties or warranties imposed by law, including merchantability or fitness for any particular purpose.

Please note that these rights do not automatically extend to content, data or other material published by Springer Nature that may be licensed from third parties.

If you would like to use or distribute our Springer Nature journal content to a wider audience or on a regular basis or in any other manner not expressly permitted by these Terms, please contact Springer Nature at

onlineservice@springernature.com